Article

Fullerene Negative Ions: Formation and Catalysis

Zineb Felfli, Kelvin Suggs, Nantambu Nicholas and Alfred Z. Msezane *

Department of Physics and CTSPS, Clark Atlanta University, Atlanta, GA 30314, USA; zfelfli@cau.edu (Z.F.);
kelvlorenz@yahoo.com (K.S.); nantambu.nicholas@students.cau.edu (N.N.)
* Correspondence: amsezane@cau.edu

check for
updates

Abstract: We first explore negative-ion formation in fullerenes C_{44} to C_{136} through low-energy electron elastic scattering total cross sections calculations using our Regge-pole methodology. Then, the formed negative ions C_{44}^- to C_{136}^- are used to investigate the catalysis of water oxidation to peroxide and water synthesis from H_2 and O_2. The exploited fundamental mechanism underlying negative-ion catalysis involves hydrogen bond strength-weakening/breaking in the transition state. Density Functional Theory transition state calculations found C_{60}^- optimal for both water and peroxide synthesis, C_{100}^- increases the energy barrier the most, and C_{136}^- the most effective catalyst in both water synthesis and oxidation to H_2O_2.

1. Introduction

To celebrate the International Year of the Periodic Table, the Royal Society of Chemistry published the themed collection 'Single Atoms as Active Catalysts' [1]. This has motivated the present investigation of using single fullerene molecular anions as catalysts. Toward this end, we first investigate the formation of negative ions in the fullerene molecules C_{44}, C_{60}, C_{70}, C_{98}, C_{112}, C_{120}, C_{132}, and C_{136} through low-energy electron elastic scattering total cross sections (TCSs) calculations. Our robust Regge-pole methodology is used for the calculations. The formed anionic fullerenes C_{44}^- to C_{136}^- during the collisions are then used to investigate the catalysis of water oxidation to peroxide and water synthesis from H_2 and O_2. Negative ion catalysis involves anionic molecular complex formation in the transition state, with the atomic negative ion weakening/breaking the hydrogen bond strength. This is the same fundamental mechanism that underlies the well-investigated muon-catalyzed nuclear fusion using a negative muon, a deuteron, and a triton; it has been proposed to drive nanoscale catalysis [2,3]. Specifically, in the experiments [4–6], the fundamental atomic mechanism responsible for the oxidation of water to peroxide catalyzed by Au and Pd nanoparticles has been attributed to the interplay between Regge resonances and Ramsauer–Townsend (R-T) minima in the electron elastic TCSs for the Au and Pd atoms, along with their large electron affinities (EAs) [2,3].

The mechanism of negative-ion catalysis has been demonstrated in the oxidation of H_2O to H_2O_2 catalyzed using the Au^- and Pd^- anions to understand the experiments of Hutchings and collaborators [4–6], in the catalysis of light, intermediate and heavy water to the corresponding peroxides [7], and in the oxidation of methane to methanol without the CO_2 emission [8] to name a few. Briefly, the experiments [4–6] synthesized hydrogen peroxide from H_2 and O_2 using supported on Fe_2O_3 Au, Pd, and Au-Pd nanoparticles as catalysts. Importantly, these experiments found that the addition of Pd to the Au catalyst increased the rate of H_2O_2 synthesis significantly as well as the concentration of the formed H_2O_2. In [4], it was found that the production of H_2O_2 increased 7- and 30-fold over that of the Au catalyst alone when using the Pd and Au-Pd, respectively. Recently,

the experiment [6] used the less expensive atomic Sn catalyst for possible water purification in the developing world. Consequently, here we explore the effectiveness of the fullerene negative ions C_{44}^- to C_{136}^- in the catalysis of water oxidation to peroxide and water synthesis from H_2 and O_2 in search of less expensive catalysts. The focus is particularly on the larger fullerene molecules greater than C_{70}.

The importance of fullerene molecules in negative ion catalysis, organic solar-cells, sensor technology, drug delivery, catalytic efficiency in fundamental hydrogenation, etc., has motivated us to study the variation of the EA with the fullerene size from C_{44} to C_{136} and contrast the EAs with that of the standard C_{60}. Manifesting the existence of long-lived negative ion formation, reliable atomic, and molecular affinities are crucial for understanding the vast number of chemical reactions involving negative ions [9]. In the formation of fullerene negative ions, it has been demonstrated for the first time that the ground state anionic binding energies (BEs) extracted from our Regge-pole calculated TCSs for the C_{20} through C_{92} fullerenes matched excellently the measured EAs [10–17]. This provides a novel and general approach to the determination of reliable EAs for complex heavy systems. Indeed, the EAs provide a stringent test of theoretical calculations when their results are compared with those from reliable measurements. In addition, the Regge-pole methodology requires no assistance whatsoever from either experiment or other theory for the remarkable feat. The results [18,19] provided great credence to the power and ability of the Regge-pole methodology to extract reliable EAs of the fullerene molecules from the calculated ground states electron elastic TCSs. It is noted here that obtaining unambiguous and reliable fullerene EAs is a challenging task for existing theoretical methods. Generally, the Regge-pole calculated low-energy electron elastic TCSs for fullerene molecules are characterized by ground, long-lived polarization-induced metastable, and excited negative ion formation.

Except for the C_{60} fullerene, theoretical and/or experimental low-energy electron elastic scattering TCSs for fullerenes are generally sparse. For C_{60}, low-energy electron scattering cross sections have been investigated theoretically [20–27]. Very recently, angle-differential electron elastic scattering from C_{60} has been studied [28]. The investigations of Wigner Time Delay in electron-C_{60} elastic scattering [29] using potential models defined by the fullerene EA and its radius will certainly benefit from this study. Experimentally, low-energy electron elastic scattering differential cross sections for C_{60} were measured [30]. Gas phase fullerenes C_{76} and C_{78} [31] and gas phase C_{60} and C_{70} [32] have been studied using low-energy electron scattering. In the latter study, several resonant states were identified including the determination of the lifetimes of the formed negative ions. Thermal rate coefficients and cross sections for electron attachment to C_{60} have been studied [33] including their low energy temperature dependence in a crossed electron beam–molecular beam experiment [34].

The low-energy electron elastic collision TCSs of the fullerene molecules obtained in this paper as well as those of the already studied fullerenes [18,19,35,36] and the actinide [37] and the lanthanide [38,39] atoms should contribute to a better understanding of the role of the individual atoms/fullerenes in ongoing studies involving endohedral systems [40–46]. Additionally, expected to benefit from this study will be the exploration of the M@C_{60} (M = Ti, Zr,U) fullerene hybrids that have demonstrated catalytic efficiency in fundamental hydrogenation [47].

2. Results

In Section 2.1 we first present the variation with the electron impact energy E of the Regge-pole calculated electron elastic scattering TCSs for the fullerene molecules C_{44} to C_{136}. Section 2.2 demonstrates the utility of the fullerene molecular anions in the catalysis of water oxidation to peroxide and water synthesis from H_2 and O_2 using the anionic fullerene catalysts C_{44}^- to C_{136}^-.

2.1. Fullerene Electron Scattering Total Cross Sections

In fullerene negative ion formation, it has been demonstrated for the first time that the ground state anionic BEs extracted from our Regge-pole calculated electron elastic scattering TCSs for the C_{20} through C_{92} fullerenes matched excellently the measured EAs of these fullerenes [18,19]. This provides a novel and general approach to the determination of unambiguous and reliable EAs for complex heavy

systems. The Regge-pole methodology requires no assistance whatsoever from either experiment or other theory to achieve the remarkable feat.

Figures 1 and 2 present the elastic TCSs for the fullerene molecules C_{44} through C_{136} and Table 1 summarizes the essential data. Indeed, the Regge-pole calculated low-energy electron elastic TCSs for the fullerene molecules considered here are found to be characterized generally by ground, polarization-induced metastable and excited negative ion formation. For ground state collisions the resultant anionic BEs yield the theoretically challenging to calculate EAs and demonstrate their wide variation from fullerene to fullerene. The results here are consistent with the observation that low-energy electron-fullerene interactions are generally characterized by rich resonance structures [32,48–50] and that the experimentally detected fullerene isomers correspond to the metastable states [51]. They also support the conclusion that the EAs of fullerene molecules are relatively large [52]. This should satisfy part of the requirement to increase fullerene acceptor resistance to degradation by the photo-oxidation mechanism as well as improve the understanding of the degradation mechanism in organic solar cells [53]. The determined EAs here could also be employed to construct the widely used simple model potentials for the fullerene shells, including endohedral fullerenes [54]. The resonance-rich structures of the fullerene TCSs and their large EAs explain the tendency of fullerenes to form compounds with electron-donor anions and their vast applications as well. These TCSs require careful delineation and identification of the attendant resonance structures for reliable interpretation as well as extraction of the EAs.
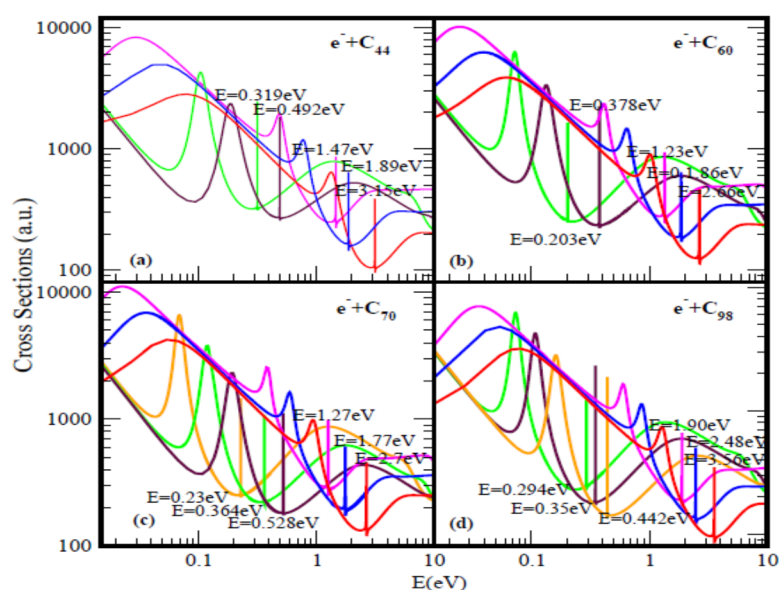

Figure 1. Total cross sections (a.u.) for (**a**) C_{44}, (**b**) C_{60}, (**c**) C_{70} and (**d**) C_{98}. The red, blue and pink curves represent total cross sections (TCSs) for the ground and induced metastable states (first and second), respectively. The green and brown curves in (**a**) and (**b**) denote the TCSs for the first and the second excited states, respectively. For C_{70} and C_{98} the orange, green and brown curves represent the excited states TCSs. The dramatically sharp resonances correspond to the fullerene anions formed during the collisions.
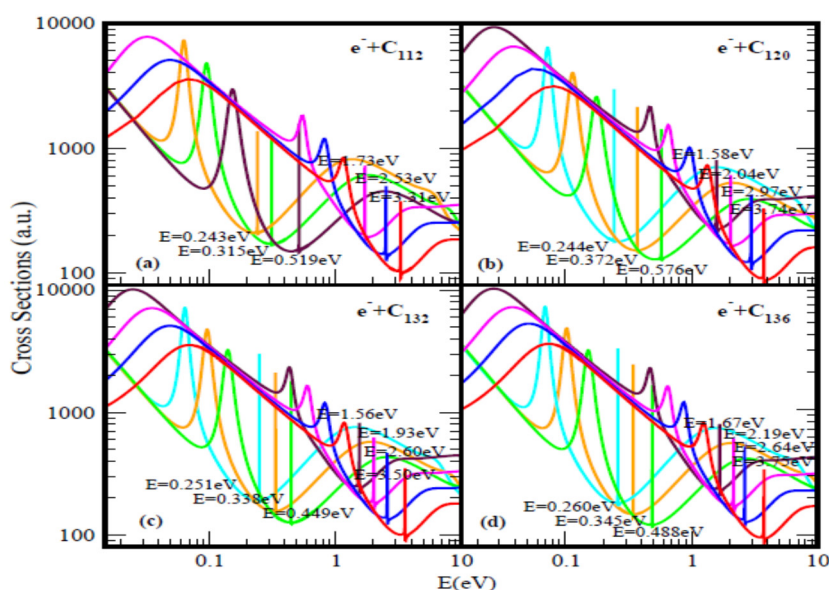
Figure 2. Total cross sections (a.u.) for (**a**) C_{112}, (**b**) C_{120}, (**c**) C_{132} and (**d**) C_{136}. The red, blue, pink and brown (no brown curve for C_{112}) curves represent TCSs for the ground and induced metastable states (first, second and third), respectively. For C_{112} (orange, green and brown), while for C_{120}, C_{132} and C_{136} (light blue, orange and green) curves correspond to the excited TCSs. The dramatically sharp resonances correspond to the anions formed during the collisions.

Table 1. Fullerene ground (GR-S), metastable (MS-n, n = 1, 2, 3) and first excited (EXT-1), second excited (EXT-2) and third excited (EXT-3) anionic states binding energies (BEs). R-T refers to the energy position of the ground state R-T minimum. The measured EAs are represented as Expt. All the energies are in eV.

Full.	Bes GR-S	BEs MS-1	BEs MS-2	BEs MS-3	BEs EXT-1	BEs EXT-2	BEs EXT-3	R-T GR-S	EA Expt.
C_{44}	3.15	1.89	1.47	-	0.319	0.492	-	3.13	3.30 [15]
C_{60}	2.663 [19] 2.57 [55] 2.23 [56] 2.63 [57]	1.86	1.23	-	0.203	0.378	-	2.68	2.65 [10] 2.666 [12] 2.664 [58] 2.684 [11]
C_{70}	2.70	1.77	1.27	-	0.230	0.364	0.528	2.72	2.676 [12] 2.72 [14] 2.765 [13] 2.74 [59]
C_{98}	3.56	2.48	1.90	-	0.294	0.350	0.442	3.54	-
C_{112}	3.31	2.53	1.73	-	0.243	0.315	0.519	3.32	-
C_{120}	3.74	2.97	2.04	1.58	0.244	0.372	0.576	3.73	-
C_{132}	3.59	2.60	1.93	1.56	0.251	0.338	0.449	3.58	-
C_{136}	3.75	2.64	2.19	1.67	0.260	0.345	0.488	3.77	-

For a better appreciation of the physics underlying the resonance-rich TCSs for the various fullerenes presented in the Figures 1 and 2, we first discuss briefly the TCSs for the C_{44} fullerene. With less structure, the TCSs were first calculated in [18]; here they have been recalculated to expose more resonances. It is noted that generally the internal region of zero potential provided by the hollow cage structure of the fullerenes is conducive to metastable anionic formation during the collisions. This is clearly manifested through the appearance of additional resonances in the TCSs as the fullerene size increases from C_{44} through C_{136}. Also, this explains the existence of the two series of resonances,

the first is associated with the ground state TCS while the second belongs to the highest excited state TCS (green curve).

Focusing specifically on the C_{44} TCSs, Figure 1a, the red, blue, pink, brown and green curves represent respectively the TCSs of the ground; the first & the second metastable and the two excited states. The fundamental physics underlying these curves can be readily understood if we focus on each color-coded TCS. For the analysis we select the ground state TCS curve, the red curve. Near threshold the TCS exhibits the characteristic shape resonance (SR), broad maximum. As the electron energy is increased, the fullerene becomes polarized and reaches maximum polarization manifested through the appearance of the first R-T minimum at about 1.01 eV, indicative that the polarization interaction has been accounted for adequately in the calculation [60]. With further increase in the electron impact energy, the electron becomes trapped by the centrifugal potential, demonstrated by the appearance of the SR at 1.41 eV. As the electron leaks out of the centrifugal potential, the C_{44} shell, due to its strong polarizability, becomes significantly polarized leading to the generation of the second deep R-T minimum in the TCS at 3.13 eV. At the absolute minimum the long-lived ground state of the C_{44}^- anion is formed with the BE of 3.15 eV. At the R-T minimum the electron spends many angular rotations about the C_{44} as it decays; the angular life is determined by $1/[\text{Im }\lambda_n(E)] \rightarrow \infty$, since for the ground state resonance $\text{Im }\lambda_n(E) \rightarrow 0$, see Equation (1). Notably, at the R-T minimum new molecules can be created from fermions.

The analysis is also applicable to the other fullerene TCSs presented in Figure 1 as well as in Figure 2. The extracted BEs of the negative ions formed during the collisions are summarized in Table 1 where they are compared with available EAs. Indeed, for the ground state collisions the extracted from the TCSs anionic BEs correspond to the EAs of the fullerenes. The Regge-pole calculated TCSs for the C_{60} fullerene presented in Figure 1b is taken from [39]. The TCSs, typical of those calculated in this paper, are found to be characterized generally by dramatically sharp resonances manifesting ground, metastable and excited anionic formation during the collisions, Ramsauer-Townsend (R-T) minima and shape resonances. Indeed, the ground state TCS (red curve) yields the anionic BE, located at its absolute R-T minimum; it has been identified with the C_{60} EA [19]. Viewed as presented in the Figure 1b the C_{60} TCSs appear complicated as well. However, they are readily understood and interpreted as was done in [19,39]. This ground state TCS is clearly shown alone in Figure 1 of [19] and the underlying physics is also presented there.

Figures 1b and 2 demonstrate the variation of the electron TCSs with E for the C_{60}, C_{70}, C_{98}, C_{112}, C_{120}, C_{132} and C_{136} fullerene molecules. Clearly, these TCSs are characterized as in the C_{44} case by ground, metastable and excited anionic formation, R-T minima and shape resonances. The extracted anionic BEs from the ground states TCSs correspond to the EAs of the fullerene molecules. These BEs, presented in Table 1 demonstrate their wide variation from fullerene to fullerene. The various dramatically sharp resonances in the TCSs represent negative ion formation in the ground, metastable and excited states.

2.2. Fullerene Transition State Barriers

The utility of the fullerene negative ions has been demonstrated in the catalysis of water oxidation to peroxide and water synthesis from H_2 and O_2 using the anionic fullerene catalysts C_{44}^- to C_{136}^-. The reactions of interest are:

Water Oxidation to Peroxide Reaction:

$$2H_2O + O_2 \rightarrow 2H_2O_2; \tag{1}$$

Water Synthesis Reaction:

$$2H_2 + O_2 \rightarrow 2H_2O. \tag{2}$$

Reaction (1) is similar to Equation (1) of Ref. [2] where the active catalyst is the Au^- anion. The processes considered here are exactly similar to that, except that here the Au^- anion catalyst is

replaced by the C_{44}^- to C_{136}^- anion catalysts. We will therefore use the familiar Au^- anion catalyst to explain and demonstrate the importance of the transition state (TS) in the reactions. Additionally, in the end, we will simply replace the Au^- with the C_{44}^- to C_{136}^- anion catalysts. Since the final product, viz. Equation (4) of Ref [2] is devoid of the catalyst as it should, we look at the transition states, Equation (2), and Equation (1). In the oxidation of H_2O to H_2O_2 catalyzed by the Au^- anion, the anion–molecular complex $Au^-(H_2O)_{1,2}$ is formed in the TS. This complex subsequently breaks up into Au^- and $(H_2O)_1$ and $(H_2O)_2$. The large EA of atomic Au played an essential role in the process. It is important in the dissociation energy of the complex $Au^-(H_2O)_{1,2}$ into the above products. The need in negative ion catalysis for systems with reliable EAs is now evident. In the present calculation, we simply replace the Au^- anion catalyst with the fullerene anion catalysts.

Figures 3 and 4 demonstrate the Density Functional Theory (DFT) calculated transition states. DFT and dispersion corrected DFT approaches have been employed for the transition state evaluations. Geometry optimization of the structural molecular conformation utilized the gradient-corrected Perdew-Burke-Ernzerhof parameterizations [61] of exchange-correlation as implemented in DMol3 [62]. A tolerance of 1×10^{-3} Ha was used with a smearing value of 0.005 Ha. DFT calculated energy barriers reduction in the oxidation of H_2O to H_2O_2 catalyzed using the anionic fullerene catalysts C_{44}^- to C_{136}^- are shown in Figure 3. Results in Figure 4 are for the water synthesis from H_2 and O_2 catalyzed using the anionic fullerene catalysts C_{44}^- to C_{136}^- as well.

DFT transition state calculations found the C_{52}^- and C_{60}^- anions to be numerically stable for both water oxidation and water synthesis and the C_{100}^- anion to increase the energy barrier the most in the water synthesis from H_2 and O_2. When catalyzing both water oxidation to peroxide and synthesis from H_2 and O_2, the C_{136}^- anion has proved to be the most effective in reducing the energy barrier significantly. Importantly, a single large fullerene such as the C_{136}, C_{120}, or even the C_{70} could replace the Au, Pd, and Sn atoms in the catalysis of H_2O_2 from H_2O in the experiments of Hutchings and collaborators [4–6] acting as a multiple-functionalized catalyst. These fullerenes have their metastable BEs close to the EAs of the used atoms in the experiments. Thus, an inexpensive dynamic water purification system for the developing world could be realized [6].
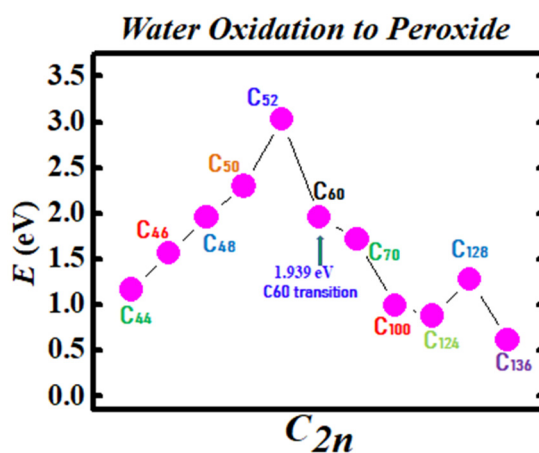

Figure 3. Transition state calculation of anionic fullerenes C_{44}^- to C_{136}^- catalyzing water oxidation to peroxide.
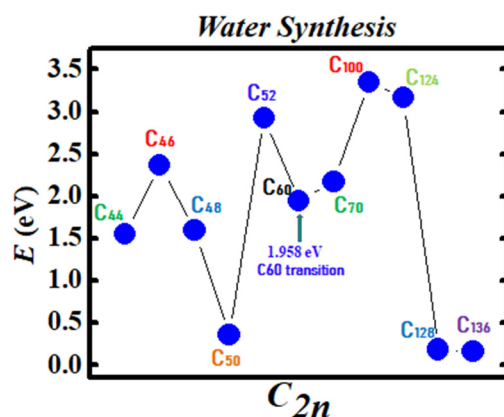
Figure 4. Transition state calculation of anionic fullerenes C_{44}^- to C_{136}^- catalyzing oxygen and hydrogen synthesis to water.

3. Method of Calculation

In [63] it was confirmed that Regge poles formed during low-energy electron elastic scattering become stable bound states. Here we adopt the Regge-pole methodology, also known as the complex angular momentum (CAM) method for the calculation of the electron scattering TCSs. Regge poles, singularities of the S-matrix, rigorously define resonances [64,65]. Being generalized bound states, they can be used to calculate reliably the anionic BEs of the ground, metastable and excited states of complex heavy systems through the TCSs calculations. The Mulholland formula [66] is used here to calculate the near-threshold electron–fullerene collision TCS resulting in negative ion formation as resonances. In the form below, the TCS fully embeds the essential electron-electron correlation effects [67,68] (atomic units are used throughout):

$$\sigma_{tot}(E) = 4\pi k^{-2} \int_0^\infty Re[1 - S(\lambda)]\lambda d\lambda - 8\pi^2 k^{-2} \sum_n Im \frac{\lambda_n \rho n}{1 + \exp(-2\pi i \lambda_n)} + I(E) \tag{3}$$

In Equation (3) $S(\lambda)$ and λ are respectively the S-matrix and the CAM, $k = \sqrt{2mE}$, m being the mass and E the impact energy, ρ_n is the residue of the S-matrix at the nth pole, λ_n and $I(E)$ contains the contributions from the integrals along the imaginary λ-axis; its contribution has been demonstrated to be negligible [69].

As in [26] the complicated details of the electronic structure of the fullerene itself are not considered here. The incident electron is assumed to interact with the complex atom/fullerene through the Thomas-Fermi type potential, known as the Avdonina, Belov and Felfli (ABF) potential [70] which accounts for the vital core-polarization interaction

$$U(r) = \frac{Z}{r(1 + \alpha z^{\frac{1}{3}} r)(1 + \beta z^{\frac{2}{3}} r^2)} \tag{4}$$

In Equation (4) Z is the nuclear charge, α and β are variation parameters. This potential has the appropriate asymptotic behavior, *viz.* $\sim -1/(\alpha\beta r^4)$ and accounts properly for the polarization interaction at low energies. This potential, extensively studied [71], has five turning points and four poles connected by four cuts in the complex plane. The presence of the powers of Z as coefficients of r and r^2 in Equation (4) ensures that spherical and non-spherical atoms/fullerenes are correctly treated. The effective potential $V(r) = U(r) + \lambda(\lambda + 1)/2r^2$ is considered here as a continuous function of the variables r and complex λ. The details of the numerical evaluations of the TCSs have been described in [68] and further details of the calculations may be found in [72].

In the calculations, the optimal value of α was determined to be 0.2. When the TCS as a function of β has a dramatically sharp resonance [69], corresponding to the formation of a stable negative

ion, this resonance is longest lived for a given value of the energy, which corresponds to the EA of the system (for ground state collisions) or the BE of the metastable/excited anion. Also calculated in the CAM methods are the Regge Trajectories, viz. *Im* $\lambda_n(E)$ versus *Re* $\lambda_n(E)$; they have been used to demonstrate that at low energy relativistic and non-relativistic calculations yield the same results [73].

4. Conclusions

The Regge-pole calculated low-energy electron elastic TCSs for the fullerene molecules considered here are found to be characterized generally by ground, metastable, and excited negative ion formation. Indeed, the rich resonance structures of the fullerenes TCSs and their large EAs explain the tendency of fullerenes to form compounds with electron-donor anions and their vast applications as well.

The utility of the formed negative ions has been demonstrated in the catalysis of water oxidation to peroxide and water synthesis from H_2 and O_2 using the anionic fullerene catalysts C_{44}^- to C_{136}^-. Transition state calculations using DFT found the C_{52}^- and C_{60}^- anions to be robust (yielding essentially the same transition state energies) for both water and peroxide synthesis and the C_{136}^- to be the most effective in reducing the energy barrier significantly. Importantly, a single large fullerene such as the C_{136}, C_{120}, or even the C_{60} could replace the Au, Pd, and Sn atoms in the catalysis of H_2O_2 from H_2O in the experiments [4–6] acting as a multiple-functionalized catalyst. Thus, an inexpensive dynamic water purification system could be realized through the use of fullerene anions as catalysts. Furthermore, these fullerenes could also be used as catalysts in the production of methanol from methane without carbon dioxide emission with significant impact on the environment.

Author Contributions: Conceptualization, methodology, investigation, formal analysis and writing of the original draft as well as rewriting and editing were carried out by A.Z.M. He is also responsible for securing the funding for the research. Z.F. was responsible for the theoretical calculations of the electron scattering total cross sections for the fullerene molecules, acquisition of the corresponding data and plotting as well as tabulating them. K.S. conceptualized the fullerene negative ion catalysis and calculated the transition state energy barriers of the fullerene molecules. He also plotted the relevant figures. N.N. assisted in collecting the references and organized them. He also helped in the calculation of the transition states of the fullerenes. All authors have read and agreed to the published version of the manuscript.

Conflicts of Interest: The authors declare no conflict of interest or state.

References

1. International Year of the Periodic Table: Single Atoms as Active Catalysts. Available online: https://pubs.rsc.org/en/journals/articlecollectionlanding?sercode=nr&themeid=1fc90a67-e081-4265-99eb-2201eb17c286 (accessed on 12 January 2017).
2. Msezane, A.Z.; Felfli, Z.; Sokolovski, D. Novel mechanism for nanoscale catalysis. *J. Phys. B* **2010**, *43*, 201001. [CrossRef]
3. Msezane, A.Z.; Felfli, Z.; Sokolovski, D. Cold fusion mechanism in nanoscale catalysis. *Europhys News* **2010**, *41*, 11.
4. Edwards, J.K.; Carley, A.F.; Herzing, A.A.; Kiely, C.J.; Hutchings, G.J. Direct synthesis of hydrogen peroxide from H2 and O2 using supported Au–Pd catalysts. *J. Chem. Soc. Faraday Discuss* **2008**, *138*, 225. [CrossRef]
5. Edwards, J.K.; Solsona, B.; Landon, P.; Carley, A.F.; Herzing, A.; Watanabe, M.; Kiely, C.J.; Hutchings, G.J. Direct synthesis of hydrogen peroxide from H2 and O2 using Au–Pd/Fe2O3 catalysts. *J. Mater. Chem.* **2005**, *15*, 4595. [CrossRef]
6. Freakley, S.J.; He, Q.; Harrhy, J.H.; Lu, L.; Crole, D.A.; Morgan, D.J.; Ntainjua, E.N.; Edwards, J.K.; Carley, A.F.; Borisevich, A.Y.; et al. Palladium-tin catalysts for the direct synthesis of H2O2 with high selectivity. *Science* **2016**, *351*, 959. [CrossRef]

7.   Tesfamichael, A.; Suggs, K.; Felfli, Z.; Wang, X.-Q.; Msezane, A.Z. Atomic Gold and Palladium Negative-Ion Catalysis of Light, Intermediate, and Heavy Water to Corresponding Peroxides. *J. Phys. Chem. C* **2012**, *116*, 18698. [CrossRef]

8.   Msezane, A.Z.; Felfli, Z.; Tesfamichael, A.; Suggs, K.; Wang, X.-Q. Gold anion catalysis of methane to methanol. *Gold Bulletin* **2012**, *3*, 127. [CrossRef]

9.   Kasdan, K.; Lineberger, W.C. Alkali-metal negative ions. II. Laser photoelectron spectrometry. *Phys. Rev. A* **1974**, *10*, 1658. [CrossRef]

10.   Wang, L.-S.; Conceicao, J.J.; Jin, C.M.; Smalley, R.E. Threshold photodetachment of cold C−60. *Chem. Phys. Lett.* **1991**, *182*, 5. [CrossRef]

11.   Huang, D.-L.; Dau, P.D.; Liu, H.T.; Wang, L.-S. High-resolution photoelectron imaging of cold C_{60}^- anions and accurate determination of the electron affinity of C_{60}. *J. Chem. Phys.* **2014**, *140*, 224315. [CrossRef]

12.   Brink, C.; Andersen, L.H.; Hvelplund, P.; Mathur, D.; Voldstad, J.D. Laser photodetachment of C60− and C70− ions cooled in a storage ring. *Chem. Phys. Lett.* **1995**, *233*, 52. [CrossRef]

13.   Wang, X.B.; Woo, H.K.; Huang, X.; Kappes, M.M.; Wang, L.S. Direct Experimental Probe of the On-Site Coulomb Repulsion in the Doubly Charged Fullerene Anion C_{70}^{2-}. *Phys. Rev. Lett.* **2006**, *96*, 143002. [CrossRef]

14.   Boltalina, O.V.; Sidorov, L.N.; Sukhanova, E.V.; Skokan, E.V. Electron affinities of higher fullerenes. *Rapid Commun. Mass Spectrom.* **1993**, *7*, 1009.

15.   Kietzmann, H.; Rochow, R.; Gantefor, G.; Eberhardt, W.; Vietze, K.; Seifert, G.; Fowler, P.W. Electronic structure of small fullerenes: Evidence for the high stability of C32. *Phys. Rev. Lett.* **1998**, *81*, 5378. [CrossRef]

16.   Wang, X.-B.; Woo, H.-K.; Yang, J.; Kappes, M.M.; Wang, L.S. Photoelectron Spectroscopy of Singly and Doubly Charged Higher Fullerenes at Low Temperatures: C76-, C78-, C84- and C762-, C782-, C842-. *J. Phys. Chem. C* **2007**, *111*, 17684. [CrossRef]

17.   Boltalina, O.V.; Ioffe, I.N.; Sorokin, I.D.; Sidorov, L.N. Electron Affinity of Some Endohedral Lanthanide Fullerenes. *J. Phys. Chem. A* **1997**, *101*, 9561. [CrossRef]

18.   Msezane, A.Z.; Felfli, Z. New insights in low-energy electron-fullerene interactions. *Chem. Phys.* **2018**, *503*, 50. [CrossRef]

19.   Felfli, Z.; Msezane, A.Z. Simple method for determining fullerene negative ion formation. *Euro. Phys. J. D* **2018**, *72*, 78. [CrossRef]

20.   Winstead, C.; McKoy, V. Elastic electron scattering by fullerene, C60. *Phys. Rev. A* **2006**, *73*, 012711. [CrossRef]

21.   Lucchese, R.R.; Gianturco, F.A.; Sanna, N. Low-energy electron scattering from C60 molecules. *Chem. Phys. Lett.* **1999**, *305*, 413. [CrossRef]

22.   Gianturco, F.A.; Lucchese, R.R.; Sanna, N. Computed elastic cross sections and angular distributions of low-energy electron scattering from gas phase C60 fullerene. *J. Phys. B* **1999**, *32*, 2181. [CrossRef]

23.   Gianturco, F.A.; Lucchese, R.R. One-particle resonances in low-energy electron scattering from C60. *J. Chem. Phys.* **1999**, *111*, 6769. [CrossRef]

24.   Ipatov, A.N.; Ivanov, V.K.; Pacheco, J.M.; Ekardt, W. Exchange and polarization effects in elastic electron scattering by metallic clusters. *J. Phys. B* **1998**, *31*, L5119. [CrossRef]

25.   Dolmatov, V.K.; Cooper, M.B.; Hunter, M.E. Electron elastic scattering off endohedral fullerenes A@ C60: The initial insight. *J. Phys. B* **2014**, *47*, 15002. [CrossRef]

26.   Dolmatov, V.K.; Amusia, M.Y.; Chernysheva, L.V. Effects of target polarization in electron elastic scattering off endohedral A@C60. *Phys. Rev. A* **2017**, *95*, 012709. [CrossRef]

27.   Amusia, M.Y.; Chernysheva, L.V. On the behavior of scattering phases in collisions of electrons with multiatomic objects. *JETP Letters* **2015**, *101*, 503. [CrossRef]

28.   Amusia, M.Y.; Chernysheva, L.V.; Dolmatov, V.K. Angle-differential elastic-electron scattering off C 60: A simple semi-empirical theory versus experiment. *J. Phys. B* **2019**, *52*, 085201. [CrossRef]

29.   Amusia, M.Y.; Baltenkov, A.S. Time delay in electron-C60 elastic scattering in a dirac bubble potential model. *J. Phys. B* **2019**, *52*, 015101. [CrossRef]

30.   Tanaka, H.; Boesten, L.; Onda, K.; Ohashi, O. Crossed-Beam Experiment for the Scattering of Low Energy Electrons from Gas Phase C60. *J. Phys. Soc. Jpn.* **1994**, *63*, 485. [CrossRef]

31.   Elhamidi, O.; Pommier, J.; Abouaf, R.J. Low energy electron impact on C76 and C84: Excitation, metastable anion formation, and lifetime. *Int. J. Mass Spectr.* **2001**, *205*, 17. [CrossRef]

32. Elhamidi, O.; Pommier, J.; Abouaf, R.J. Low-energy electron attachment to fullerenes and in the gas phase. *J. Phys B* **1997**, *30*, 4633. [CrossRef]

33. Viggiano, A.A.; Friedman, J.F.; Shuman, N.S.; Miller, T.M.; Schaffer, L.C.; Troe, J. Experimental and modeling study of thermal rate coefficients and cross sections for electron attachment to C60. *J. Chem. Phys.* **2010**, *132*, 194307. [CrossRef] [PubMed]

34. Prabhudesai, V.S.; Nandi, D.; Krishnakumar, E. Low energy electron attachment to C60. *Euro Phys. J. D* **2005**, *35*, 261. [CrossRef]

35. Msezane, A.Z.; Felfli, Z.; Shaginyan, V.R.; Amusia, M.Y. Anionic formation in low-energy electron scattering from large fullerenes: Their multiple functionalization. *Int. J. Current Adv. Research* **2017**, *6*, 8503–8509.

36. Msezane, A.Z.; Felfli, Z. Low-energy electron scattering from fullerenes and heavy complex atoms: Negative ions formation. *Eur. Phys. J. D* **2018**, *72*, 173. [CrossRef]

37. Felfli, Z.; Msezane, A.Z. Negative Ion Formation in Low-Energy Electron Collisions with the Actinide Atoms Th, Pa, U, Np and Pu. *Appl. Phys. Res.* **2019**, *11*, 52. [CrossRef]

38. Felfli, Z.; Msezane, A.Z. Conundrum in Measured Electron Affinities of Complex Heavy Atoms. *J. At. Mol. Condens. Nano Phys.* **2018**, *5*, 73. [CrossRef]

39. Msezane, A.Z. Negative Ion Binding Energies in Complex Heavy Systems. *J. At. Mol. Condens. Nano Phys.* **2018**, *5*, 195. [CrossRef]

40. Ryzhkov, M.V.; Ivanovskii, A.L.; Delley, B. Electronic structure and stabilization of c60 fullerenes encapsulating actinide atom. *Nanosyst. Phys. Chem. Math.* **2014**, *5*, 494.

41. Ryzhkov, M.V.; Ivanovskii, A.L.; Delley, B. Electronic structure of endohedral fullerenes An@ C28 (An = Th–Md). *Comp. Theor. Chem.* **2012**, *985*, 46. [CrossRef]

42. Ryzhkov, M.V.; Delley, B. Electronic structure of predicted endohedral fullerenes An@ C40 (An = Th–Md). *Comp. Theor. Chem.* **2013**, *1013*, 70. [CrossRef]

43. Popov, A.A.; Yang, S.; Dunsch, L. Endohedral Fullerenes. *Chem. Rev.* **2013**, *113*, 5989–6113. [CrossRef] [PubMed]

44. Wang, Y.; Morales-Martínez, R.; Zhang, X.; Yang, W.; Wang, Y.; Rodríguez-Fortea, A.; Poblet, J.M.; Feng, L.; Wang, S.; Chen, N. Unique Four-Electron Metal-to-Cage Charge Transfer of Th to a C82 Fullerene Cage: Complete Structural Characterization of Th@C3v(8)-C82. *J. Am. Chem. Soc.* **2017**, *139*, 5110. [CrossRef] [PubMed]

45. Jin, P.; Lin, C.; Li, Y.; Li, L.; Zhao, Y. Th@C76. Computational characterization of larger actinide endohedral fullerenes. *Int. J. Quant. Chem.* **2018**, *118*, e25501. [CrossRef]

46. Dunk, P.W.; Kaiser, N.K.; Mulet-Gas, M.; Rodriguez-Fortea, A.; Poblet, J.M.; Shinohara, H.; Hendrickson, C.L.; Marshall, A.G.; Kroto, H.W. The Smallest Stable Fullerene, M@C28 (M = Ti, Zr, U): Stabilization and Growth from Carbon Vapor. *J. Am. Chem. Soc.* **2012**, *134*, 9380. [CrossRef] [PubMed]

47. Vital, S.; Marco-Martinez, J.; Filippone, S.; Martin, N. Fullerenes for catalysis: Metallofullerenes in hydrogen transfer reactions. *Chem. Commun.* **2017**, *53*, 4842. [CrossRef] [PubMed]

48. Lezius, M.; Scheier, P.; Mark, T.D. Free electron attachment to C60 and C70. *Chem. Phys. Lett.* **1993**, *203*, 232. [CrossRef]

49. Jaffke, T.; Illenberger, E.; Lezius, M.; Matejcik, S.; Smith, D.; Mark, T.D. Formation of C60− and C70− by free electron capture. Activation energy and effect of the internal energy on lifetime. *Chem. Phys. Lett.* **1994**, *226*, 213. [CrossRef]

50. Huang, J.; Carman, H.S.; Compton, R.N. Low-Energy Electron Attachment to C60. *J. Phys. Chem.* **1995**, *99*, 1719. [CrossRef]

51. Kronik, L.; Fromherz, R.; Ko, E.; Ganteför, G.; Chelikowsky, J.R. Highest electron affinity as a predictor of cluster anion structures. *Nat. Mater.* **2002**, *1*, 49. [CrossRef]

52. Hoke, E.T.; Sachs-Quintana, I.T.; Lloyd, M.T.; Kauvar, I.; Mateker, W.R.; Nardes, A.M.; Peters, C.H.; Kopidakis, N.; McGehee, M.D. The role of electron affinity in determining whether fullerenes catalyze or inhibit photooxidation of polymers for solar cells. *Adv. Energy Mat.* **2012**, *2*, 13. [CrossRef]

53. Mateker, W.R.; McGehee, M.D. Progress in Understanding Degradation Mechanisms and Improving Stability in Organic Photovoltaics. *Adv. Mater.* **2016**. [CrossRef] [PubMed]

54. Baltenkov, A.; Manson, S.T.; Msezane, A.Z. Jellium model potentials for the C60 molecule and the photoionization of endohedral atoms, A@C60. *J. Phys. B* **2015**, *48*, 185103. [CrossRef]

55. Nagase, S.; Kabayashi, K. Theoretical study of the lanthanide fullerene CeC82. Comparison with ScC82, YC82 and LaC82. *Chem. Phys. Lett.* **1999**, *228*, 106. [CrossRef]

56. Tarento, R.J.; Joyes, P.Z. Size dependence of the electronic and magnetic properties of fullerenes (C60-C240). *Phys. D* **1996**, *37*, 165. [CrossRef]

57. Zakrzewski, V.G.; Dolgounitcheva, O.; Ortiz, J.V. Electron Propagator Calculations on the Ground and Excited States of C_{60}^-. *J. Phys. Chem. A* **2014**, *118*, 7424. [CrossRef]

58. Støchkel, K.; Andersen, J.U. Photo excitation and laser detachment of C60− anions in a storage ring. *J. Chem. Phys.* **2013**, *139*, 164304. [CrossRef]

59. Palpant, B.; Otake, A.; Hayakawa, F.; Negishi, Y.; Lee, G.H.; Nakajima, A.; Kaya, K. Photoelectron spectroscopy of sodium-coated C60 and C70 cluster anions. *Phys. Rev. B* **1999**, *60*, 4509. [CrossRef]

60. Johnson, W.R.; Guet, C. Elastic scattering of electrons from Xe, Cs+, and Ba2+. *Phys. Rev. A* **1994**, *49*, 1041. [CrossRef]

61. Tkatchenko, A.; Scheffler, M. Accurate Molecular Van Der Waals Interactions from Ground-State Electron Density and Free-Atom Reference Data. *Phys. Rev. Lett.* **2009**, *102*, 73005. [CrossRef]

62. DMol3 2011 Accelrys Software Inc.: San Diego, CA.

63. Hiscox, A.; Brown, B.M.; Marletta, M. On the low energy behavior of Regge poles. *J. Math. Phys.* **2010**, *51*, 102104. [CrossRef]

64. Frautschi, S.C. *Regge Poles and S-matrix Theory*; W. A. Benjamin, Inc.: New York, NY, USA, 1963; Chapter X. [CrossRef]

65. D'Alfaro, V.; Regge, T.E. *Potential Scattering*; Amsterdam: Amsterdam, The Netherlands, 1965.

66. Mulholland, H.P. An asymptotic expansion for Σ(2n+1)exp (Àσ(n+1/2)2). *Proc. Camb. Phil. Soc. (London)* **1928**, *24*, 280–289. [CrossRef]

67. Macek, J.H.; Krstic, P.S.; Ovchinnikov, S.Y. Regge Oscillations in Integral Cross Sections for Proton Impact on Atomic Hydrogen. *Phys. Rev. Lett.* **2004**, *93*, 183203. [CrossRef] [PubMed]

68. Sokolovski, D.; Felfli, Z.; Ovchinnikov, S.Y.; Macek, J.H.; Msezane, A.Z. Regge oscillations in electron-atom elastic cross sections. *Phys. Rev. A* **2007**, *76*, 012705. [CrossRef]

69. Felfli, Z.; Msezane, A.Z.; Sokolovski, D. Resonances in low-energy electron elastic cross sections for lanthanide atoms. *Phys. Rev. A* **2009**, *79*, 012714. [CrossRef]

70. Felfli, Z.; Belov, S.; Avdonina, N.B.; Marletta, M.; Msezane, A.Z.; Naboko, S.N. *Proceedings of the Third International Workshop on Contemporary Problems in Mathematical Physics*; Govaerts, J., Hounkonnou, M.N., Msezane, A.Z., Eds.; World Scientific: Singapore, 2004; pp. 218–232.

71. Belov, S.; Thylwe, K.-E.; Marletta, M.; Msezane, A.Z.; Naboko, S.N. On Regge pole trajectories for a rational function approximation of Thomas–Fermi potentials. *J. Phys. A* **2010**, *43*, 365301. [CrossRef]

72. Burke, P.G.; Tate, C. A program for calculating regge trajectories in potential scattering. *Comp. Phys. Commun.* **1969**, *1*, 97. [CrossRef]

73. Thylwe, K.W. On relativistic shifts of negative-ion resonances. *Eur. Phys. J. D* **2012**, *66*, 7. [CrossRef]